WATER MELTING AND SOLIDIFICATION CONSIDERING THE NATURAL CONVECTION IN POLAR GEOMETRY

Sandi Itamar Schäfer de Souza
Universidade Regional Integrada do Alto Uruguai e das Missões – DECC – GIESS
Av. Universidade das Missões 464, 98802-470 - Santo Ângelo, RS.
sandi@urisan.tche.br

Horácio Antonio Vielmo
Universidade Federal do Rio Grande do Sul - Depto de Engenharia Mecânica – GESTE
R. Sarmento Leite 425, 3° andar, 90050-170 - Porto Alegre, RS.
vielmoh@mecanica.ufrgs.br

Abstract. *In order to domain the energy storage technology in the form of latent heat it is necessary to solve the melting and solidification problems of a phase change material (PCM). This work describes efforts in finding solutions that more closely approach the physical reality of the problem. Simulations for the partial melting, with a new solidification in sequence, and for the solidification of pure water in the interior of cylinders are presented. Inversion of the density is taken into account. The simulations have been developed in the transient form, using the Finite Volume Method for the solution of the governing equations. The solutions are optimized concerning the mesh and time steps. The behavior of the solid-liquid interface geometry, the field of enthalpy and density in the domain, the streamlines and the behavior of the Rayleigh number are presented as the result of the solutions found. Comparisons between the solid volume when considering only the diffusive process and when considering the convective process are carried through. The behavior of the bulk temperature of the liquid is also evaluated for the two forms of solution. The grid convergence index is applied (GCI) for the verification of grid independence.*

Keywords*. Phase Change, Melting and Solidification, Ice Banks, Finite Volumes, Cylindrical Geometry.*

1. Introduction

Latent heat energy storage systems become of capital importance when one desires to rationalize electrical energy consumption. An important application of this technology is the assistance to central air-conditioned and industrial refrigeration plants so as to lower energy consumption at its peak and to render consumption more uniform along the day. As in other countries, the cost of industrial electrical energy is variable along the day in Brazil, and one of its highest values coincides with peak moments. Another relevant factor concerning cost is contract demand which, when surpassed, causes the consumer to pay a fine. To ensure economic viability ice banks have been used to render the energy consumption curve more favorable during peak consumption. However, some undesirable aspects are associated with the usage of this technology, one of which is the uncertainties in the equation of heat transfer taxes during the melting and solidification of phase change material (PCM).

Due to the complexity of the problems of phase change material, simplifying hypotheses are usually adopted. Among these hypotheses, the one which disrespects the effects of natural convection has had the highest impact. When the PCM is water, the effects of density inversion are usually disregarded, following the classical approaches of Stefan and Neumman. One of the most used configurations in ice banks is PCM confinement in tubes. Fusion and internal solidification were dealt with by Saitoh and Hirose (1982), who presented numerical solutions, by Rieger et all (1983), who experimentally and numerically investigated paraffin melting, by Ho and Viskanta (1984), who also carried out experimental and numerical research using paraffin as PCM, and by Hirata and Nishida (1989) who, too, used paraffin in their experimental investigations. One of the first researches to use water as PCM in tubes was the one by Rieger et all (1986), who carried out experimental investigation. Tsai and Hwang (1998), developed numeric and experimental studies in duct flow, taking into consideration the effects of density variation. Chen and Lee (1998) developed experimental studies on the melting process taking metastability into consideration. This work uses first-order boundary conditions to simulate melting, and it resorts to melting with water sequential resolidification in a cylindrical geometry. The effects of density inversion and of the effects of natural convection were taken into consideration. The practical problem focused here is a latent heat storage module. It consists of a sheaf of tubes with pure water as PCM, which resorts to internal cross flow. Only one tube is considered in this approach.

2. Physical model and boundary conditions

Domain geometry, as well as its nomenclature, is shown in Fig. (1).

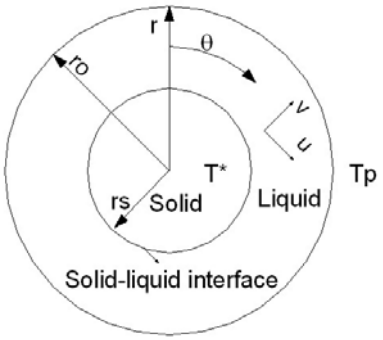

Figure 1. Physical Model

First-order boundary condition, both in the melting and solidification phases, was considered to simulate this problem, as shown in the physical model in Fig. (1),

$$T(r_0,\theta) = T_p \qquad \rightarrow \qquad t > 0 \tag{1}$$

where T *(°C)* is the temperature, r_0 *(m)* the external radius, θ *(rad)* the angular positions, T_p *(°C)* the wall temperature and t *(s)* is time.

For the hydrodynamic problem, boundary conditions used were non-sliding and impermeability both in the tube and in solid PCM,

$$u = v = 0 \quad \rightarrow \quad r = r_0 \;\; e \;\; r = r_S \tag{2}$$

where u *(m/s)* is angular velocity, v *(m/s)* é radial velocity, r *(m)* radial position, r_s *(m)* solid radius.

The initial condition assumed in the solution of the thermal problem during melting depends on the approach to be used. In Stefan's approach, we have:

$$T(r,\theta) = T^* \qquad \rightarrow \qquad t = 0 \tag{3}$$

where, T^* *(°C)* is the temperature of melting, whereas in Neumann's approach,

$$T(r,\theta) = T_{Sub} \qquad \rightarrow \qquad t = 0 \tag{4}$$

In solidification initial condition will be:

$$T(r,\theta) = T_{ini} \qquad \rightarrow \qquad t = 0 \tag{5}$$

where T_{sub} *(°C)* is the temperature of sub-cooling and T_{ini} *(C°)* is the initial temperature.

For the hydrodynamic problem, both in melting and in solidification,

$$u = v = 0 \qquad \rightarrow \qquad t = 0 \tag{6}$$

3. Governing equations

Heat transfer from or to encapsulated fluid generates thermal gradients that, in turn, generate density gradients inside the fluid domain. In the presence of a gravitational field, under certain physical configurations, density gradients may cause movement and, therefore, the existence of natural or free convection. According to the literature, the treatment given to the cavity is applied to a large number of natural phenomena and industrial processes associated with melting and solidification. Exemplifying, one may mention the melting and solidification of an encapsulated PCM in spheres, plates or tubes, where the internal solid surface is mobile (solid-liquid interface). Following this reasoning, knowledge of the fields of velocity, temperature, density and pressure is needed to the full solution of this kind of problems, which characterizes a linkage between the thermal and hydrodynamic problems, and makes it necessary that

the governing equations be solved simultaneously. Governing equations for this geometry are written below for the polar coordinates system.

3.1. Continuity equation

$$\frac{\partial \rho}{\partial t}+\frac{1}{r}\frac{\partial\left(r\rho v\right)}{\partial r}+\frac{1}{r}\frac{\partial\left(\rho u\right)}{\partial \theta}=0 \tag{7}$$

where ρ *(kg/m³)* represents density.

3.2. Movement quantity equations in the directions *r* and θ

$$\left(\frac{\partial\left(\rho v\right)}{\partial t}+\frac{1}{r}\frac{\partial\left(r\rho v^2\right)}{\partial r}+\frac{1}{r}\frac{\partial\left(\rho uv\right)}{\partial \theta}+\frac{\rho u^2}{r}\right)=-\frac{\partial p}{\partial r}+\mu\left[\frac{\partial}{\partial r}\left(\frac{1}{r}\frac{\partial\left(rv\right)}{\partial r}\right)+\frac{1}{r^2}\frac{\partial^2 v}{\partial \theta^2}+\frac{2}{r^2}\frac{\partial u}{\partial \theta}\right]+\rho B_r \tag{8}$$

$$\left(\frac{\partial\left(\rho u\right)}{\partial t}+\frac{1}{r}\frac{\partial\left(r\rho vu\right)}{\partial r}+\frac{1}{r}\frac{\partial\left(\rho u^2\right)}{\partial \theta}+\frac{\rho uv}{r}\right)=-\frac{1}{r}\frac{\partial p}{\partial \theta}+\mu\left[\frac{\partial}{\partial r}\left(\frac{1}{r}\frac{\partial\left(ru\right)}{\partial r}\right)+\frac{1}{r^2}\frac{\partial^2 u}{\partial \theta^2}+\frac{2}{r^2}\frac{\partial v}{\partial \theta}\right]+\rho B_\theta \tag{9}$$

being p *(N/m²)* pressure, B_r e B_θ the radial and an angular components of field forces, which in both cases is gravitational acceleration g *(m/s²),* and μ *(N s/m²)* dynamic viscosity. Boussinesq's approximation was adopted for the treatment of body force terms in the liquid phase, assuming reference temperature as the melting temperature $T_{ref}=T^*$ and $\rho_{ref}=\rho^*$. According to Maxwell's thermodynamical relations [Van Wylen et all (1998), Callen (1985), e Bejan (1994)] we have the equation of the thermodynamical state, which relates density to temperature and pressure for a given substance,

$$\rho=\rho(T,p) \tag{10}$$

for small mass variations it is acceptable to expand the function about a reference situation, with a Taylor series, originating:

$$\rho\cong\rho_{ref}+\left(\frac{\partial\rho}{\partial T}\right)_p\left(T-T_{ref}\right)+\left(\frac{\partial\rho}{\partial p}\right)_T\left(p-p_{ref}\right)+... \tag{11}$$

for liquids, and using the thermal expansion coefficient β, Eq. (11) assumes,

$$\rho\cong\rho_{ref}\left[1+\beta\left(T_{ref}-T\right)\right] \tag{12}$$

inserting Eq. (12) in Eq. (8) e (9) we have:

$$\left(\frac{\partial\left(\rho v\right)}{\partial t}+\frac{\partial\left(\rho v^2\right)}{\partial r}+\frac{1}{r}\frac{\partial\left(\rho uv\right)}{\partial \theta}+\frac{\rho u^2}{r}\right)=-\frac{\partial p_H}{\partial r}+\mu\left[\frac{\partial}{\partial r}\left(\frac{1}{r}\frac{\partial\left(rv\right)}{\partial r}\right)+\frac{1}{r^2}\frac{\partial^2 v}{\partial \theta^2}+\frac{2}{r^2}\frac{\partial u}{\partial \theta}\right]+\rho^* g\beta cos\theta\left(T-T^*\right) \tag{13}$$

$$\left(\frac{\partial\left(\rho u\right)}{\partial t}+\frac{\partial\left(\rho vu\right)}{\partial r}+\frac{1}{r}\frac{\partial\left(\rho u^2\right)}{\partial \theta}+\frac{\rho uv}{r}\right)=-\frac{1}{r}\frac{\partial p_H}{\partial \theta}+\mu\left[\frac{\partial}{\partial r}\left(\frac{1}{r}\frac{\partial\left(ru\right)}{\partial r}\right)+\frac{1}{r^2}\frac{\partial^2 u}{\partial \theta^2}+\frac{2}{r^2}\frac{\partial v}{\partial \theta}\right]-\rho^* g\beta sen\theta\left(T-T^*\right) \tag{14}$$

where p_H is the hydrostatic component. Due to the fact that water density does not behave in a linear form with temperature it is necessary to determine the behavior of the volumetric expansion coefficient for each discretized volume. To this end, Vasseur's et all polynomial (1983), was used to model the behavior of density according to temperature.

$$\beta=-1.9364x10^{-7}T^2+1.7507012x10^{-5}T-6.59759847x10^{-5} \tag{15}$$

4. Energy equation

In phase change problems, the domain is composed by three distinct regions, each of which having specific properties. For pure substances, temperature is constant in solid liquid interfaces. To solve this difficulty, energy equation, written considering thermodynamic property enthalpy *h (J/kg)* with constant thermal conductivity *k (W/m K)*, is used.

$$\frac{\partial(\rho h)}{\partial t}+\frac{1}{r}\frac{\partial(r\rho vh)}{\partial r}+\frac{1}{r}\frac{\partial(\rho uh)}{\partial\theta}=k\left[\frac{1}{r}\left(\frac{\partial}{\partial r}\left(r\frac{\partial T}{\partial r}\right)\right)+\frac{1}{r^2}\frac{\partial^2 T}{\partial\theta^2}\right] \tag{16}$$

Adopting Cao et al's model (1989), which used Kirchoff's concept of temperature, described and applied by Vielmo (1993), considering constant thermal conductivity in each phase,

$$T_k=\begin{cases}k_S\left(T-T^*\right) & \rightarrow h\le 0 \quad \rightarrow(Solid\ \ phase)\\ 0 & \rightarrow 0<h<\lambda \quad \rightarrow(Interface)\\ k_L\left(T-T^*\right) & \rightarrow h\ge\lambda \quad \rightarrow(Liquid\ \ phase)\end{cases} \tag{17}$$

where the sub-indices *S* and *L* refer to liquid and solid phases. Energy equation becomes:

$$\frac{\partial(\rho h)}{\partial t}+\frac{1}{r}\frac{\partial(r\rho vh)}{\partial r}+\frac{1}{r}\frac{\partial(\rho uh)}{\partial\theta}=\frac{1}{r}\left(\frac{\partial}{\partial r}\left(r\frac{\partial \mathrm{E}(h)h}{\partial r}\right)\right)+\frac{1}{r^2}\frac{\partial^2 \mathrm{E}(h)h}{\partial\theta^2}+\frac{1}{r}\left(\frac{\partial}{\partial r}\left(r\frac{\partial S(h)}{\partial r}\right)\right)+\frac{1}{r^2}\frac{\partial^2 S(h)}{\partial\theta^2} \tag{18}$$

where,

$$\begin{aligned}&\mathrm{E}(h)=\frac{k_S}{(c_p)_S} && S(h)=0 && \rightarrow h\le 0 && \rightarrow(Solid\ \ phase)\\ &\mathrm{E}(h)=0 && S(h)=0 && \rightarrow 0<h<\lambda && \rightarrow(Interface)\\ &\mathrm{E}(h)=\frac{k_L}{(c_p)_L} && S(h)=-\frac{\lambda k_L}{(c_p)_L} && \rightarrow h\ge\lambda && \rightarrow(Liquid\ \ phase)\end{aligned} \tag{19}$$

where c_p *(J/kg K)* is the specific heat and λ *(J/kg)* is the latent heat.

5. Numeric methodology

The finite volume approximation described by Patankar (1980) and Maliska (1995) was used for the discretization of the governing equations. In the treatment of movement quantity equations, the generic variable ϕ and the diffusive coefficient Γ become $\phi=u$ for the coordinate θ, $\phi=v$ for the coordinate r and $\Gamma=\mu$..

In energy depends on the focus being on the liquid, interface or solid. For the solution of this equation Patankar's algorithm was modified, taking into consideration the characteristics of Cao et al's model (1989). The algebraic equation system resulting from the integration of differential equations is solved by the TriDiagonal-Matrix Algorithm (TDMA), with block correction. The interpolation function used is *Power-Law*, and the SIMPLEC was used to treat the pressure-velocity coupling. A computational grid of *40x40* volume elements was used.

Sub-relaxations of 0.8 order were used for all variables due to the instabilities of the hydrodynamic problem. Values of the 10^{-8} order were used as convergence criteria, both for enthalpy variations and for the maximal mass residues (SMAX). The adoption of variable temporal evolutions was needed due to numerical divergences. Time steps were chosen so as that enthalpy, in the liquid domain, developed in the order of *200 J/kg*, when there were no control volumes in phase change. When there were control volumes close to phase change, time steps were reduced to values that produced enthalpy variations of the order of *10 J/kg*, in liquids. The existence of three distinct domains with specific properties for each region contributes to the complexity of the problem. To immobilize the solid region a high value was attributed to absolute viscosity, $\mu=10^{50}$, in the positions where $h<\lambda$.

6. Results and discussion

The results discussed here were calculated for a diameter *d=0.064 m*. Pure water was used as working fluid, initially in the sub-cooling solid phase (Neumann´s approach), that is, in *t=0*, T_{sub}*=-8°C;* to begin the melting process the wall tube was exposed T_p*=4°C*, as it can be seen for the instant *t=6000 s*, in Fig. (2). In *t=15000 s*, T_p*=-5.5°C* is prescribed, starting resolidification that can be identified in the instant *t=15010 s*. The symmetry of the problem was

considered for simulation, and thermal resistance imposed by the tube wall was disregarded. Enthalpy behavior in the domain is exposed on the right, in color scale with superimposed isenthalpic lines. Enthalpy value $h=0$ for solid in melting temperature, i. e, $T=T^{*}=0°C$ was used as reference value for the simulations. Therefore, negative enthalpies characterize the solid regions, whereas enthalpy values higher than latent heat identify the liquid region, $h \geq \lambda = 333472.8$ J. Phase change region has higher values for enthalpy $0<h<\lambda$. On the left corner, on the bottom, is Rayleigh number for the instant, which is defined according to Ho and Tu (1998):

$$Ra_c = \frac{\omega\, g \left(\Delta T\right)^{1.894816} \overline{L}^{3}}{\alpha\, \nu} \tag{20}$$

where ΔT in melting represents the temperature difference between the wall and melting temperature; in solidification this difference is the one between liquid average temperature and melting temperature. α (m^2/s) is thermal diffusivity, ν (m^2/s) cinematic viscosity, $\omega=9.297173x10^{-6}$ $(°C^{1.894816})$ and $\overline{L}$ (m) average thickness in the liquid region.

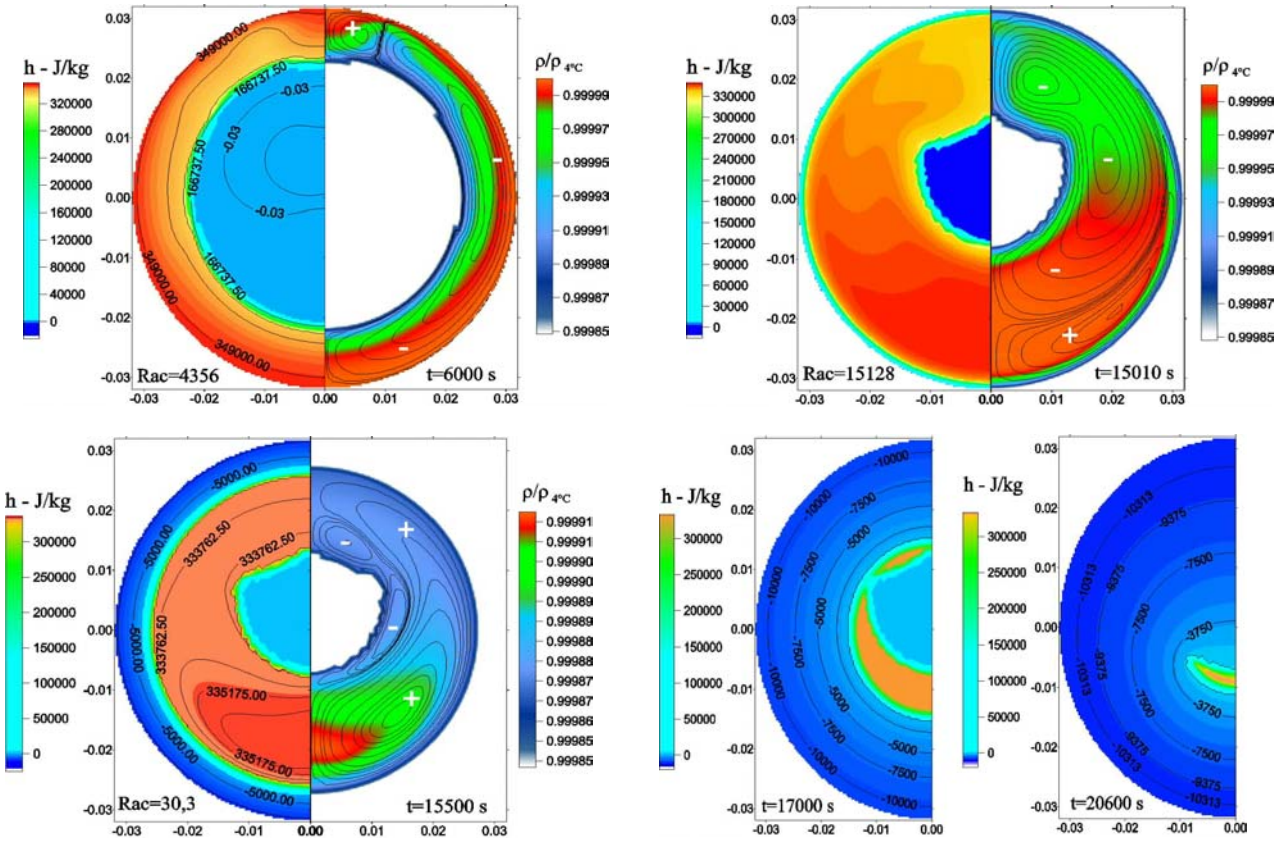

Figure 2. Numeric results for partial melting in the periods $t=6000$ s, $t=15010$ s (starting of resolidification), $t=15500$ s, $t=17000$ s, $t=20600$ s. On the left, enthalpy behavior. On the right, relative density with superimposed streamlines

Density behavior in the liquid region is exposed on the right side, in color scale. The highest value is in red, and the minimal values in blue. Streamlines are superimposed to the behavior of the relative density, enabling the observation of liquid behavior during the evolution of the phenomenon. On the bottom are exposed the times for which simulations were made. In Fig. (2), $t=6000$ s, one can observe the behavior of the melting process, and it can be seen that the fluid with the highest energy level is concentrated in the inferior regions of the tube. Since wall temperature is $T_p=4°C$, the density of the liquid, close to the wall, will reach its maximum value. This causes the movement of the liquid in these regions to the inferior levels of the tube. The liquid close to the solid will have a lower density and therefore it will go to the superior positions of the tube. This behavior is shown on the left side of the same figure, and it was repeated for the simulations with $T_p \leq 4°C$. It is possible to perceive the existence of a eddy standard that demonstrates the behavior of the phenomenon. Two eddies occur for this instant, a bigger one rotating clockwise (negative) and one rotating anti-clockwise (positive). Eddies structure is dynamic along time, and in simulations with wall temperatures $T_p \geq 8°C$ there is an inversion in the behavior of the enthalpy and density, there being a liquid concentration with higher energy in the superior position. Eddies standard is also completely altered.

In $t=15010$ s resolidification is already happening, and one can observe the existence of a thin solid layer. Concentration of fluid with high enthalpy occurs at the bottom of the tube, and from this moment on there are two phase

change fronts, the solidification front and the melting front, and the liquid is confined between them. The advance of the melting front is reduced by sensible energy associated with liquid, and this effect is more intensely felt at the bottom, generating a lack of uniformity in the thickness of the solidified material. The solid in the central position, that is in melting temperature, continues to melt until temperature balance is reached. In *t=15500 s* eddies structure is completely altered and minimized, for density gradients are very low. In *t=17000 s* there aren't density gradients any longer and the meeting of the two phase change boundaries happens; the internal solid starts to exchange diffusive energy with the solidification front, as can be seen through isenthalpic in *t=20600 s*, a situation close to complete solidification. Behavior standard in solidification depends on the liquid temperature in the beginning of the process. In simulations carried out with initial temperature $T_{ini} \geq 8°C$, a concentration of liquid with high energy occurs at the top of the tube in the beginning of the process; when the mixture temperature defined by Eq. (21) hits $T_{mist} \approx 4°C$, concentration occurs at the bottom of the tube, that tends to equalize the thickness of the solidification front. Influence of natural convection, during melting, is small at first, growing with the evolution of the phenomenon. Its effect can be noticed through the "disfigurement" of the solid in the center of the tube.

In solidification, the time and intensity of the action of natural convection are bigger for situations where initial sensible energy, brought by the temperature of the liquid T_{ini}, is elevated with a low T_p. To evaluate the importance of natural convection in the solidification process the behavior T_{mist}/T_{ini} in the relation V_{sol}/V_0, where V_{sol} is the solidified volume of PCM and V_0 is the initial volume. Fig. (3a) was plotted for two simulations. In both, the same physical model, boundary conditions and initial conditions were considered, being the difference between them the method used for their solution. The first was developed considering the process of solidification as purely diffusive, and the other with convection action.

$$T_{mist} = \frac{\left(\frac{1}{m_l} \int_{volume} h \rho \, dv \right) - \lambda}{(cp)_l} \tag{21}$$

One observes a faster decrease in T_{mist} in the simulation solved with natural convection, and this behavior was repeated in the simulations developed with other boundary and initial conditions. The intensity of the difference between the two solutions becomes smaller with the decrease of sensible energy in the liquid in the beginning of the process. The time needed for the homogenization of the temperature in the liquid domain also decreases for the same reason, and the decrease of T_{ini} causes the same effects.

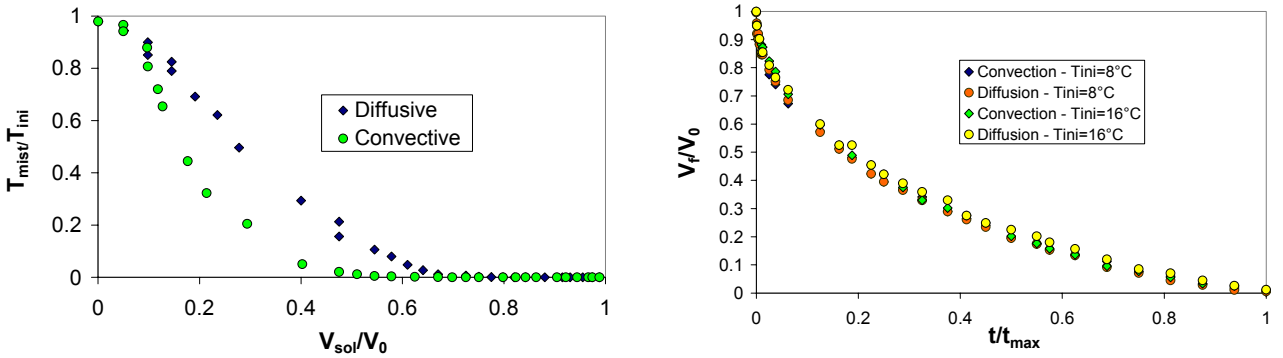

Figure 3. (a) The behavior of the relation T_{mist}/T_{ini} in the relation V_{sol}/V_0 for diffusive and convective solutions with $T_{ini}=16°C$ and $T_p=-5.5°C$. (b) The behavior of the relation V_f/V_0 in the relation t/t_{max} using $T_{ini}=8°C$ and $T_{ini}=16°C$ with $T_p=-5.5°C$. Simulations developed considering the pure diffusive process and the process in the presence of natural convection

The influence of the natural convection and of the sensible energy extant in the beginning of the process on PCM solidification time can be visualized in Fig. (3b), through the behavior of the relation V_f/V_0 in the relation t/t_{max}. There V_f is the liquid volume and t_{max} is the maximum time of the solidification process. Results for the two different situations in solidification are exposed. In the first $T_{ini}=8°C$ was considered, in the second $T_{ini}=16°C$, with $T_p=-5.5°C$ in both situations. In both cases, solutions were obtained for the pure diffusive process and for the process occurring in the presence of natural convection. When evaluating these solutions one perceives their proximity, for even there not being a faster decrease of T_{mist} when convection is not considered, this does not causes significant differences between the two solutions, the pure diffusive one and the one in the presence of natural convection. This behavior may be justified by the fact that sensible energy is much lower than latent energy, low Stefan numbers. Sensible energy level in the liquid has little interference on solidification velocity, for temperatures in the order of *8°C*, and is coincident in solutions with natural convection and pure diffusion.

For higher temperatures, as in *16°C*, solidification velocity is lower in the first instants, $V_f/V_0 > 0.6$, of the convective process. After homogenization of the temperature is reached, Fig. (3), there is an inversion in the velocities of solidification for $V_f/V_0 < 0.4$, and the convective process is more rapid for $V_f/V_0 < 0.4$. At the end of the process solidified bulk is the same for both cases and the time for this to happen, t_{max}, is similar in all simulated cases.

In order to validate these results it is necessary to evaluate associate errors, and to this end Grid Convergence Index (GCI) methodology, Roache (1998), was applied to the results of the simulations developed for melting. Neumann´s approach was used in the initial condition, $T_{ini}=-5.5°C$, and in the boundary condition $T_p=10$°C; a tube with diameter *d=60 mm* was used. Initially Eq. (22) was used to evaluate the order of the method employed. This required obtaining results in three different grid situations. The grid relation used was *r=3*, grids with *40x40*, *120x120* and *360x360* volume element number. This created the need of a geometric coincidence among the evaluated points, as well as of a temporal coincidence, which was also observed. Enthalpy was the variable chosen to verify method order *p*. It was chosen because it is the central variable of the problem. The results are in Tab. (1).

$$p = \frac{\ln\left(\frac{f_3 - f_2}{f_2 - f_1}\right)}{\ln(r)} \qquad \textbf{(22)}$$

where *f* terms are solutions and the sub-indices *1*, *2* and *3* refer to the refined, intermediate and less refined grid.

Evaluations were developed for three angular positions in the tube and, in each of these positions, three positions along the radius were chosen. The angles of these positions are referred in relation to the abscissa axes. These positions were chosen so that there would be one at the top of the tube, one in its medial position and one at its bottom. Result analysis shows that the method order was close to *1*, as it was expected, with the exception of the control volumes near the walls of the tube. In these regions velocity tends to zero, and diffusion prevails. At the inferior regions velocity decreases, causing the phenomenon to be more diffusive than convective. In these positions there is also a decreasing in the method order.

Table 1. Results for relative error and the GCI for first-order boundary conditions $T_p=10°C$, initial condition $T_i=-5.5°C$ and $r_0=30$ *mm*. *40x40*, *120x120* and *360x360* volume grids

	Position		Enthalpy h (J/kg)			Order *p*	$f_2=f_{40}$ $f_1=f_{120}$		$f_2=f_{40}$ $f_1=f_{360}$		$f_2=f_{120}$ $f_1=f_{360}$	
(s)	$X=r\cos\theta$ *(m)*	$Y=r\sin\theta$ *(m)*	Grid *40x40*	Grid *120x120*	Grid *360x360*		ε %	*GCI* %	ε %	*GCI* %	ε %	*GCI* %
200	Angular Position $\theta_1=83.25°$											
	0.00348205	0.02941965	369821.3	369763.7	369665.9	0.48	0.0156	0.066	0.041	0.18	0.025	0.11
	0.00339389	0.02867485	358094.3	358026.3	357806.3	1.07	0.018	0.024	0.079	0.1	0.06	0.08
	0.00330574	0.02793005	345959.9	345916.4	345735.6	1.2	0.013	0.014	0.065	0.07	0.051	0.056
	Angular Position $\theta_1=11.25°$											
	0.02905576	0.00577955	369771.7	369710.4	369608.9	0.46	0.016	0.073	0.043	0.2	0.026	0.12
	0.02832017	0.00563323	358002.2	357910.1	357677.8	0.84	0.026	0.051	0.091	0.18	0.065	0.13
	0.02758459	0.00548692	345903.1	345835.6	345641.2	0.96	0.019	0.03	0.076	0.11	0.056	0.09
	Angular Position $\theta_1=-83.25°$											
	0.00348205	-0.0294196	369697.7	369633.7	369527.7	0.46	0.0173	0.08	0.045	0.2	0.029	0.13
	0.00339389	-0.0286748	357864.2	357743.5	357494.7	0.66	0.034	0.096	0.099	0.28	0.07	0.2
	0.00330574	-0.0279300	345818.9	345720.3	345506.5	0.7	0.028	0.08	0.09	0.25	0.062	0.17

Evaluations of the relative error, ε, used Eq. (23),

$$\varepsilon = \frac{f_2 - f_1}{f_1} \qquad \textbf{(23)}$$

GCI was determined by using Eq. (24), considering local approximation order, *p*, Eq.(22),

$$GCI = \varepsilon\big|_{r=2}^{p=2} = 3\frac{|\varepsilon|}{r^p - 1} \tag{24}$$

As it can be seen, maximum relative error, ε, reached values of the order of *0.1%*, in comparisons between the results obtained by the *40x40* and *360x360* grids. For the GCI, the maximum error is of the order of *0.3%*, in the same situation. Based on the results shown in Tab. (1) one can say that the *40x40* volume grid was enough for the present analyses. Besides, the grid relation between the two solutions is *r=9*, representing a high computational cost for a difference of only *0.1%* in the values of the solutions.

No changes in the solution patterns were registered in all the solutions, obtained with different grids. Verification of the presence of a multiplicity of solutions was investigated through the alteration in TDMA sweepings. Sweepings were used in the coefficients and in the variables of all orientations, and no alteration in the solutions was found.

In order to validate the results of the present work, the experimental results of Rieger et all (1986) can be used. Comparisons between solutions obtained with the present methodology and experimental solutions were carried out in Souza and Vielmo (2000). It must be considered that the experimental validation of the problems focused in this work is difficult, by the scarcity of works like this in the literature. Finally the methodology of Cao et al. (1989), applied here, was also used and tested for Vielmo (1993).

7. Conclusion

In melting, both in Stefan´s and in Neumann´s approach, heat transfer occurs first through diffusion. Along the evolution of the process, thermal gradient and space in the liquid region increase. This promotes an increase in the Rayleigh number, intensifying natural convection, which becomes, in some processes, the major mechanism in heat transfer. In solidification the process occurs first in the presence of natural convection, once in this class of problem there are high thermal gradients in the beginning of the process, characterizing an initial prevalence of natural convection. Along temporal evolution, thermal gradients and the spaces filled up in the liquid decrease, causing a reduction in the Rayleigh number which renders diffusion, after a certain period, the major heat transfer mechanism, Fig. (2), for *Rac=30.3*. As it was expected, the major mechanism for heat transfer in the interior of the tube varies along time and according to boundary conditions. Eddy structure, which is variable according to time and boundary conditions, drastically interferes in the modification of the heat exchange mechanism.

The degree of complexity of the heat transfer phenomenon in these problems is associated with the “abnormal” behavior of density in water. This behavior is responsible for the variations in eddies structures and in the form of isotherms inside the tube. In melting these structures “collect” energy along the wall, delivering it to the solid, which intensifies the exchange mechanism in specific positions where fluid with low enthalpy is concentrated. Eddies structures influence phase change boundary. While diffusive process prevails, solid preserves a cylindrical geometric form, and phase change boundary geometry suffers “deformations” with the intensification of the eddies structures.

In the processes of solidification and resolidification, heat transfer to the interior of the tube also varies along time. Convective process prevails initially, due to movement in the liquid. In the initial moments eddy structures are dynamic, due to the high gradients in temperature and density. As the process evolves, gradients decrease until being extinguished. In solidification, with full liquid volume at the beginning of the process, gradient survival time depends on the initial condition, T_{ini}, and of the boundary condition T_p. In resolidification this period depends on the boundary condition, T_p, in the beginning of the processes of melting and resolidifition, and on the volume of liquid PCM. In solutions that consider only diffusion results for the solidification process are closer to reality than in those that consider melting. This happens due to the behavior of sensible energy, which increases in melting along the evolution of the process, whereas the opposite happens in solidification.

In melting, cylindrical geometric form is preserved in problems solved with pure diffusion, and constant prescribed wall temperature. This shows the distancing between the modeling and the physical reality of the problem when simplifying hypothesis, which disregard internal convection and the “abnormal” behavior of density in water, are used. In solidification the geometric form of the solid ring does not suffer major deformations, which indicates the small influence of natural convection in solidification.

It can be said that, in solidification, the solution developed only in the presence of diffusion generates acceptable results for the simulated temperature levels. Therefore, one should resort to an analytic solution of the governing equations of the problem, so as to obtain a closed-form solution to the problem.

8. Acknowledgement

The authors thank the Brazilian nation which, through CAPES – PICD program made this work possible.

9. References

Bejan, A., 1996, “Transferência de Calor”, Ed. Edgard Blücher Ltda, São Paulo – SP, Brazil, 540 p.

Callen Herbert B., 1985, “Thermodynamics and an Introduction to Thermostatistics”, John Wiley & Sons, New York, USA, 493 p.

Cao, Y., Faghri, A., Chang, W.S., 1989, “A Numerical Analysis of Stefan Problems for Generalized Multi-Dimensional Phase-Change Structures Using the Enthalpy Transforming Model”, Int. J. of Heat and Mass Transfer, vol.32, pp. 1289–1298.

Chen, Sih-Li, Lee, Tzong-Shing, 1998, “A Study of Supercooling Phenomenon and Freezing Probability of Water Inside Horizontal Cylinders”, Int. J. of Heat and Mass Transfer, vol.41, n° 4-5, pp. 769-783.

Hirata, T., Nishida, K., 1989, “An Analysis of Heat Transfer Using Equivalent Thermal Conductivity of Liquid Phase During Melting Inside an Isothermally Heated Horizontal Cylinder”, Int. J. of Heat and Mass Transfer, vol.32, n° 9, pp. 1663–1670.

Ho, C.J., Viskanta, R., 1984, “Heat Transfer During Inward Melting in a Horizontal Tube”, Int. J. of Heat and Mass Transfer, vol. 27, n° 5, pp. 705–716.

Maliska, Clovis R., 1995, “Transferência de Calor e Mecânica dos Fluidos Computacional”, LTC, Rio de Janeiro, RJ, Brazil, 424 p.

Patankar, S.V., 1980, “Numerical Heat Transfer and Fluid Flow”, McGraw-Hill, New York.

Rieger, H., Beer, H., 1986, “The Melting Process of Ice Inside a Horizontal Cylinder: Effects of Density Anomaly”, Journal of Heat Transfer, vol. 108, pp. 166-173.

Rieger, H., Projahn, U., Bareiss M., Beer, H., 1983, “Heat Transfer During Melting Inside a Horizontal Tube”, Journal of Heat Transfer, vol.105, pp. 226-234.

Roache, Patrick J., 1998, “Verification and Validation in Computational Science and Engineering”, Hermosa Publishers, New Mexico, USA, 446 p.

Saitoh, T., Hirose, K., 1982, “High Rayleigh Number Solutions to Problems of Latent Heat Thermal Energy Storage in a Horizontal Cylinder Capsule”, Journal of Heat Transfer, vol.104, pp. 545–553.

Souza, S.I.S., Vielmo, H.A., 2000, “Simulation of the Process of Melting of a MMF in Polar Geometry in the Presence of Natural Convection”, VIII ENCIT/MERCOFRIO 2000, Porto Alegre, RS, Brazil.

Tsai, C.W., Yang, S.J., Hwang, G.J., 1998, “Maximum Density Effect on Laminar Water Pipe Flow Solidification”, Int J. of Heat and Mass Transfer, vol.41, pp. 4251–4257.

Vasseur P., Robillard, L., Shekar, Chandra B., 1983, “Natural Convection Heat Transfer of Water within a Horizontal Cylindrical Annulus with Density Inversion Effects”, Journal of Heat Transfer, vol.105, pp. 117-123.

Vielmo, Horácio A., 1993, “Simulação Numérica da Transferência de Calor e Massa na Solidificação de Ligas Binárias”, Doctoral Dissertation, GPGEM/UFSC, Florianópolis, SC, Brazil.

Wylen, V., Sonntag, R.E., Borgnakke, C., 1998, “Fundamentos da Termodinâmica”, Edgard Blücher, São Paulo, SP, Brazil, 535 p.